On the ionization and dissociative photoionization of iodomethane: a definitive experimental enthalpy of formation of CH_3I

Andras Bodi,*[a] Nicholas S. Shuman†[b] and Tomas Baer[b]

Received 28th July 2009, Accepted 18th September 2009
First published as an Advance Article on the web 16th October 2009
DOI: 10.1039/b915400k

The dissociative photoionization onset energy of the $CH_3I \rightarrow CH_3^+ + I$ reaction was studied at the vacuum ultraviolet (VUV) beamline of the Swiss Light Source (SLS) using a new imaging photoelectron photoion coincidence (iPEPICO) apparatus operating with a photon resolution of 2 meV and a threshold electron kinetic energy resolution of about 1 meV. Three previous attempts at establishing this value accurately, namely a pulsed field ionization (PFI)-PEPICO measurement, *ab initio* calculations and a mass-analyzed threshold ionization (MATI) experiment, in which the onset energy was bracketed by state-selected excitation to vibrationally excited $^2A_1$ A states of the parent ion, have yielded contradictory results. It is shown that dimers and adducts formed in the supersonic molecular beam affected the PFI-PEPICO onset energy. The room temperature iPEPICO experiment yields an accurate 0 K onset of 12.248 ± 0.003 eV, from which we derive a $\Delta_f H^o_{298\ K}(CH_3I) = 15.23 \pm 0.3$ kJ mol^{-1}, and the C–I bond energy in CH_3I is 232.4 ± 0.4 kJ mol^{-1}. The room temperature breakdown diagram shows a fine structure that corresponds to the threshold photoelectron spectrum (TPES) of the A state. Low internal energy neutrals seem to be preferentially ionized in the A state when compared with the X state, and A state peaks in the TPES are Stark-shifted as a function of the DC field, whereas the dissociative photoionization of X state ions is not affected. This suggests that there are different competing mechanisms at play to produce ions in the A state *vs.* ions in the X state. The competition between field ionization and autoionization in CH_3I is compared with that in Ar, N_2 and in the H-atom loss energy region in CH_4^+. The binding energies of the neutral and ionic Ar–CH_3I clusters were found to be 26 and 66 meV, respectively.

Introduction

The measurement of dissociative photoionization onsets with an accuracy of 1 meV (0.1 kJ mol^{-1}) is one of the few methods capable of keeping pace with state of the art *ab initio* calculations[1–3] of thermochemical properties of small molecules and ions. All determinations, whether experimental or theoretical, provide only energy differences between two states. Thus, in a commonly used theoretical approach, the heat of atomization is calculated using the final atomic heats of formation as the anchor. Without the luxury of transforming a molecule into its gas phase atoms, the experimental approach is more limited and must use a variety of anchors. For example, the equilibrium constant of a neutral reaction is measured as a function of temperature, and the reactant and product enthalpies can be related to each other by means of the van't Hoff equation. In addition to neutral thermochemical cycles, various ion cycles, including processes such as $AB + h\nu \rightarrow A^+ + B + e^-$, are a welcome avenue for identifying systematic errors in neutral measurements, and complement them by the inclusion of different anchor species. However, this requires that ionic reaction heats be measured precisely and accurately. Photoelectron photoion coincidence (PEPICO) techniques are capable of measuring the dissociative photoionization onset energies to this level of precision[4–7] if both the photon and the photoelectron energies are known to within 1 or 2 meV. The dissociative photoionization of iodomethane, CH_3I, produces a methyl ion and an iodine atom in the 12.1–12.3 eV photon energy range. Because the heats of formation of both CH_3^+ and I are well established, it is possible to use these products as anchors for determining the heat of formation of the iodomethane molecule in the gas phase.

The dissociation onset for CH_3I^+ to produce the methyl ion has been studied previously by numerous groups. Tsai *et al.*[8] reported a 0 K onset of 12.25 ± 0.03 eV using the PEPICO technique with a room temperature sample. Traeger and McLaughlin[9] reported a 298 K photoionization onset of 12.18 eV. More recently, Song *et al.*[10] used a high resolution PFI-PEPICO approach[11] to determine a 0 K onset of 12.269 ± 0.003 eV with iodomethane cooled in an Ar seeded molecular beam. In parallel with these photoionization experiments, a number of groups, starting in 1977 with Morrison and co-workers,[12,13] followed by Walter *et al.*,[14] and culminating in a recent series of papers by the Kim group,[15–17]

[a] *Paul Scherrer Institut, Villigen 5232, Switzerland. E-mail: andras.boedi@psi.ch*
[b] *Department of Chemistry, University of North Carolina, Chapel Hill, NC 27599*
† Current address: Air Force Research Laboratory, Space Vehicles Directorate, 29 Randolph Road, Hanscom Air Force Base, MA 01731-3010.

prepared the iodomethane ion in its ground electronic state and photodissociated the ion to the CH_3^+ product. The combination of a cold sample and a high-resolution laser resulted in sharp photodissociation structure associated with the low frequency vibrational modes (*e.g.* the C–I stretch) of the $^2A_1$ A state of CH_3I^+ beginning at 19417 cm^{-1} relative to the electronic ground state ion and extending up to 23 500 cm^{-1}, corresponding to the 11.945–12.452 eV one-photon energy range.[15] Because the dissociation limit of the $CH_3^+ + I$ states lies at about 22 000 cm^{-1}, the photodissociation action spectroscopy proceeds *via* a 2 photon absorption from the X state for photon energies below the dissociation energy and one photon absorption above it. Hence, it is readily possible to bracket the dissociation limit between two well-isolated vibrational states of the A state, based on the required laser intensities to produce the methyl ion product. On the basis of these spectra, Lee and Kim[15] provided lower and upper limits for the dissociation limit of the iodomethane ion of 12.235 and 12.251 eV, respectively (relative to the ground state neutral molecule). It is evident that the onset of 12.269 ± 0.003 eV reported by Song *et al.*[10] is well above the Lee and Kim upper limit. Benchmark *ab initio* calculations[6] are also easier to reconcile with the photodissociation action spectroscopy brackets.

In view of the discrepancy between the Song *et al.*[10] and the Lee and Kim[15] results, we have undertaken a study using the newly constructed imaging PEPICO experiment[4] at the Swiss Light Source. Furthermore, it is of considerable interest to determine if accurate onsets can indeed be determined when a dissociation limit lies in-between sparsely-spaced quantum states of the ion, as is the case for iodomethane.

Experimental approach

The iPEPICO apparatus has been presented elsewhere[4,18] and only a brief overview is given here. A room temperature gas phase sample was introduced to the experimental chamber through an effusive source. In order to ascertain that thermal equilibrium is reached, no needle is used and the sample gas exits a 30 cm-long 6 mm outer diameter Teflon tube near the ionization region. The typical pressure outside the μ-metal shield was 5×10^{-6} to 1×10^{-5} mbar during measurement. In a second set of experiments, 2.5% iodomethane was premixed with argon or neon and supersonically cooled in a molecular beam using backing pressures from 0.3 to 3 bar. The gas was expanded through 30 or 50 μm nozzles from Agar Scientific having thicknesses of 100 μm and 2 mm, respectively. The molecular beam entered the experimental chamber through a Beam Dynamics Model 2 nickel skimmer *ca.* 5 mm from the nozzle, and arrived at the ionization region 10 cm further downstream. The background pressures in the source and in the experimental chambers were typically 1–5×10^{-4} and 5×10^{-6} mbar, respectively. The molecular beam is aimed at a Leybold 1500CL cryopump, and the experimental chamber is also pumped by an off-axis 500 l s^{-1} Pfeiffer turbomolecular pump. It is possible to check the thermal background contribution to the signal by closing the gate valve of the off-axis turbomolecular pump in the experimental chamber (which leads to an increase in the thermal background, but leaves the molecular beam density at the ionization region unchanged) and extrapolating to zero background pressure. The sum of two Gaussians may also be used to fit the Ar^+ time-of-flight (TOF) peak to determine the ratio of the molecular beam signal and the thermal background. The latter showed that 88% of the sample density in the ionization region is in the molecular beam.

The sample was ionized by the incident synchrotron radiation with a spot size of 2×4 mm at the X04DB bending magnet beamline of the Swiss Light Source.[19] The photon energy was calibrated against well-known Ar11s′–14s′ and Ne 13s′, 14s′, 12d′ and 13d′ autoionization lines, both in the 1st and 2nd order.[20] The photoelectrons are velocity map-imaged onto a DLD40 Roentdek position sensitive delay-line detector with a kinetic energy resolution better than 1 meV at threshold. The ions are extracted by the same, typically 40 V cm^{-1} field in a 5 cm-long acceleration region and then are further accelerated to −550 V to space focus them at a Jordan TOF C-726 microchannel plate detector. Ions produced in the molecular beam travel in the beam direction at a speed determined by the backing gas, *i.e.* at 560 m s^{-1} for Ar and 790 m s^{-1} for Ne. The actual offset of the ion beam at the detector may be larger than implied by the time of flight due to their crossing several grids at an acute angle. Hence, the second ion acceleration plate is split so that different voltages may be applied to each half of the plate in order to steer the ions onto the detector.

Because the electrons are imaged according to their off-axis momentum, some energetic (hot) electrons are detected in the central spot, thereby contaminating the true threshold electrons. The hot electrons are accounted for by subtracting signal collected in a small ring around the central spot with typical inner and outer diameters of 0.8 and 1–1.5 mm, respectively. This approach to hot electron subtraction was introduced by Sztáray and Baer,[21] and has also been incorporated by Garcia *et al.*[7] in their PEPICO experiment at the Soleil synchrotron. Using this method, it was possible to obtain the $^2P_{3/2}$ and $^2P_{1/2}$ peaks of Ar with a 2.6 and 2.3 meV full width at half maximum, respectively, which corresponds to the photon energy resolution measured by the width of the 11s′–13s′ autoionization lines.[4] Electron hit times and positions and ion hits are recorded in the triggerless mode of an HPTDC time to digital converter card, and electrons and ions are correlated on-the-fly to obtain time-of-flight distributions without dead time. This multiple-start/multiple-stop data acquisition scheme[18] enables data acquisition at ionization rates in excess of 100 kHz, which is beneficial at a high intensity light source, such as the synchrotron.

The experimental data may be analyzed and plotted in several ways: the threshold electron signal as a function of the photon energy yields a threshold photoelectron spectrum (TPES); the threshold electron signal detected in coincidence with an ion in a particular TOF range yields a mass-selected TPES; and the fractional ion abundances as a function of the photon energy yield the breakdown diagram, which has the significant benefit of being independent of volatile ambient parameters such as sample pressure, photon intensity and alignment.

Spectroscopy and dissociation energetics of CH_3I^+

Fig. 1 shows the potential energy curves along the C–I bond distance for iodomethane and its ionic states. The lowest energy dissociation path to $CH_3^+ + I$ ($^2P_{3/2}$) is from the two spin orbit states of the ground potential energy surface of the ion. The A state of the ion correlates with dissociation to $CH_3 + I^+$. As pointed out by Kim and coworkers,[15–17] the interesting feature in the iodomethane ion dissociation is that the dissociation limit lies in between a sparse set of optically-accessible A state vibrational levels. Furthermore, direct excitation of high vibrational levels of the ionic ground state starting from the neutral molecule appears to be highly unlikely due to vanishingly small Franck–Condon factors. On the other hand, dissociation onsets lying in Franck–Condon gaps have routinely been measured by photoionization. Examples include various dissociation onsets in N_2O^+,[22] H_2CO^+,[23] isomers of $C_3H_4^+$,[24–26] and $CH_3COCH_3^+$.[27] Explanations for the production of high vibrational levels in Franck–Condon gaps have invoked the excitation of auto-ionizing states that can convert into high vibrational levels of the ground electronic ion state.[28,29] Chupka *et al.* have has considered the role of rotational autoionization in coupling electronic and vibrational levels in the production of threshold electrons.[29] It is therefore of interest to determine (a) if we can reach the continuum states of the ground electronic state of CH_3I^+, and (b) if such rotational effects are evident.

Room temperature breakdown diagram of CH_3I^+

The threshold photoelectron spectrum is shown in the upper part of Fig. 2. The crosses above the TPES show the location of the sharp lines reported by Lee and Kim,[15] which clearly correlate with the peaks in the lower-resolution room temperature TPES. However, unlike the photodissociation spectrum [CH_3I^+ (X) + $h\nu \rightarrow CH_3I^+$ (A) $\rightarrow CH_3^+ + I$] of Lee and Kim, which did not access the high vibrational levels of the X state, our TPES shows a large and broad background underneath the A state peaks. We attribute this background to threshold photoionization yielding rovibrationally excited ions in the X state. In the same upper panel, we show the parent and product ions collected in coincidence with threshold electrons, the sum of which constitute the TPES.

The fractional parent and daughter ion abundances as a function of the photon energy (breakdown diagram) are shown in the lower panel of Fig. 2. In constructing the parent and product ion yields and the breakdown diagram, we corrected the CH_3^+/CH_3I^+ ratios using the measured collection efficiencies for these two ions. In the room temperature experiment, the efficiencies differ only because of the considerably higher velocity with which the lighter methyl ion hits the microchannel plate ion detector. The collection efficiency, E_M, was measured in the usual manner, $E_M = C_M/S_E$, where C_M is the coincidence rate for ion M^+ at a photon energy where the M^+ signal accounts for close to 100% of photoions, and S_E is the rate of threshold electron detection. The measured efficiencies for the parent and daughter ions were 20 and 25%, respectively. The initial thermal energy distribution of the parent molecule, 80% of which resides in the rotations, is transposed onto the ion manifold, and because this is a room temperature sample, results in a wide breakdown diagram, as opposed to a step function that could be expected if only one internal energy level were populated in the neutral. That is, ions are produced with internal energy equal to $h\nu + E_{th} - IE$, where E_{th} is the initial thermal energy and IE is the adiabatic ionization energy. If the threshold ionization cross-sections and the collection efficiencies are constant over the thermal energy range, the derivative of the breakdown diagram yields the thermal energy distribution;[30] since the iodomethane cation breakdown curve is not decreasing monotonously, this is certainly not the case here. Peaks corresponding to A states in the TPES coincide with peaks in the parent ion signal (upper panel), which suggests that photoionization to the A ion state

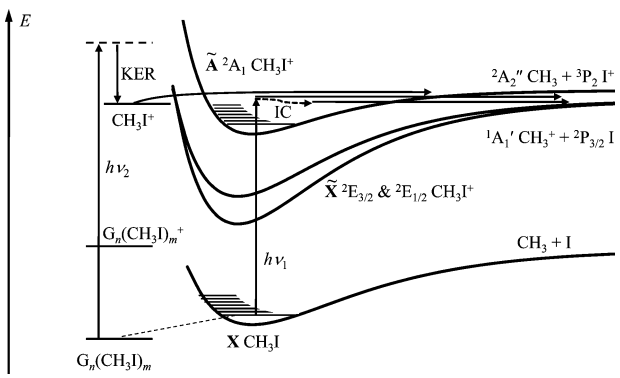

Fig. 1 CH_3I energy diagram.

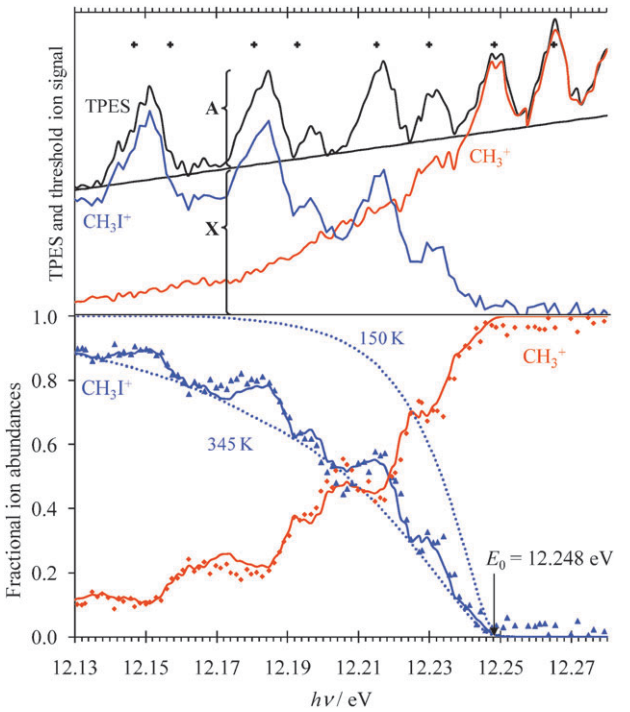

Fig. 2 Threshold electron and coincident parent and product ion signal (above), and room temperature CH_3I breakdown diagram (below). The simulated breakdown curves (continuous lines) are weighted averages of low temperature A state (150 K) and high temperature X state (345 K) breakdown curves (dotted lines). Crosses show A state peak positions based on the spectrum of Lee and Kim.[15]

produces ions with less internal energy than photoionization to the X ion state at the same photon energy. Franck–Condon factors for the transition to the ionic X and A states are markedly different, but there are two arguments against threshold ionization being governed by them. First, they are practically negligible for ionization to the vibrationally-excited X state in this energy region, whereas ions in the X state dominate the threshold ion signal. Secondly, since only 20% of the neutral thermal energy resides in the vibrations, the effect of the Frank–Condon factors on the apparent ion temperature could only be minor.

In order to gain insight into the competing transitions between neutral and ion states, we model the breakdown diagram using three parameters: the onset energy and, to characterize the internal energy distribution of the photoions, two temperatures, one for the ionic A state and one for the ionic X state. In other words, we ignore all the details about transition probabilities and assume that the X and A state ions are produced with different internal energy distributions, which we parameterize in terms of two temperatures. To determine the A to X ratio, we divided the TPES into X and A portions using the sloped solid line in the upper panel of Fig. 2. The breakdown diagram was then modeled as a linear combination of the X and A states in the proportions dictated by the TPES by varying the two assumed temperatures. The best fit was obtained using the two temperatures indicated in Fig. 2, namely 150 K for the A state and 345 K for the X state. The best fit curves produced a 0 K onset energy of 12.248 ± 0.003 eV, a value which will be discussed later.

The upper panel of Fig. 2 shows that the oscillations in the breakdown diagram originate overwhelmingly from the oscillations in the parent ion yield. Above the onset, the oscillations appear in the daughter ion intensity, but not in the breakdown diagram because the relative abundance is uniformly 100%. That the "switchover" in the oscillations from parent to daughter ion intensity is so abrupt indicates that the energy distribution of A state ions is cold, consistent with the assumed 150 K temperature found by modeling. This also precludes an alternative explanation for the oscillations in the breakdown diagram, namely that the A state ions are stabilized by, for instance, fluorescence on a time scale faster than that of internal conversion and dissociation, in which case the oscillations would remain in the parent ion intensity above the onset. Indeed, tentative fluorescence experiments did not show any increased fluorescence from the A state peaks.[31]

In our attempt at explaining the two temperatures associated with the production of X and A state ions, it must be remembered that only a small fraction of the absorption events are detected, namely those that produce threshold electrons. Other, competing processes are dissociation to neutral channels and the ejection of energetic electrons associated with the production of ground state ions in low vibrational levels. The first step in threshold ion formation has to be the Franck–Condon allowed excitation either directly to A state ions or to Rydberg states, R_A, converging to A state ions. Stark shift measurements (*vide infra*) show that A state ions are produced *via* intermediate states sufficiently long-lived to be field ionized, thereby showing that Rydberg states are involved in forming A state ions.

In order to explain the production of X state ions in the Franck–Condon gap below the A band of N_2O^+, Guyon *et al.*[28] and Chupka *et al.*[29] proposed a mechanism that is initiated by the excitation of high-n Rydberg states, R_A, converging to the various vibrational levels of the A state. This same mechanism can be applied to the CH_3I^+ dynamics. In competition with vibrational autoionization to the A state ions, the R_A can curve-cross to a neutral dissociative state, D. Once in this repulsive state, the molecule can dissociate to neutral products (*e.g.* H + CH_2I, or CH_3 + I), or it can curve-cross once more to a Rydberg state converging to the X state of the CH_3I^+ ion. Because energy must be conserved, this R_X state is highly vibrationally excited and it can autoionize by vibrational and/or rotational autoionization, yielding a threshold electron and leaving behind a vibrationally excited X state ion. The mechanism of Guyon *et al.* can be summarized as $X + h\nu \rightarrow R_A \rightarrow D \rightarrow R_X^* \rightarrow X^{+*} + e^-$, where the superscript * implies vibrational excitation. Because of the high density of A Rydberg states with various n and v quantum numbers as well as the high vibrational density of ionic states, X state ion production associated with threshold electrons can take place at any photon energy and thus be characterized by a uniform yield as shown in Fig. 2. On the other hand, **A** state ion production associated with threshold electrons can take place only at photon energies in quasi-resonance with an A state ion.

According to this model, the competition between A and X state ion production in the vicinity of an A state ion level is governed by the branching ratio between vibrational autoionization of the R_A state and curve-crossing to the dissociative D state. The curve crossing to the D state is apparently aided by rotational excitation, by an increase in the nuclear wavefunction overlap *via e.g.* centrifugal and/or Coriolis coupling. Therefore, rotationally excited R_A states will preferably cross over to a repulsive neutral state, and, consequently, end up as X state ions. This will result in preferential population of A state ions in the lower rotational states and thus be characterized by a lower A state temperature. Conversely, the X state temperature will be higher for the same reason.

To the best of our knowledge, this is the first time that such significant deviations from the neutral internal energy distribution have been observed in threshold ionization, and also the first time that competing ionization pathways are shown to have internal energy-dependent ionization cross-sections at room temperature. However, despite these effects, the derived dissociation onset energy, E_0, is independent of the internal energy distribution because, in the absence of competing parallel processes, E_0 is the energy where all parent ions have sufficient energy to dissociate and form the product ion. The onset energy is the disappearance energy of the parent ion, *i.e.* where its abundance reaches zero, 12.248 ± 0.003 eV for iodomethane. This value agrees well with the MATI-determined lower and upper limits based on state-selective excitation in the A state, and is at odds with the PFI-PEPICO value.

This onset can now be used to determine a new value for the iodomethane heat of formation. The enthalpy of formation of CH_3^+ can be determined from the very accurate methane 0 K heat of formation of -66.58 ± 0.060 kJ mol^{-1}[32] and the previously mentioned onset for CH_3^+ + H from methane

(14.323 ± 0.001 eV) reported by Weitzel *et al.*[33] Combining this with the H atom heat of formation yields a $\Delta_f H^o_{0\ K}(CH_3^+) = 1099.35 \pm 0.1$ kJ mol^{-1}. Our 12.248 eV onset for I loss from iodomethane then yields a $\Delta_f H^o_{0\ K}(CH_3I) = 24.76 \pm 0.3$ kJ mol^{-1} and a 298 K value of 15.23 ± 0.3 kJ mol^{-1}, using the B3LYP/6-311G(d,p) calculated $H_{298\ K} - H_{0\ K}$ of 10.82 kJ mol^{-1} for CH_3I. This is, within the experimental error, equal to the Pedley value of 14.4 ± 1.4 kJ mol^{-1},[34] but considerably more accurate. Based on the I loss onset and $\Delta_f H^o_{0\ K}(CH_3) = 150.0 \pm 0.3$ kJ mol^{-1},[35] it is also possible to derive the neutral $CH_3I \rightarrow CH_3 + I$ energy at 0 K, *i.e.* the C–I bond energy in iodomethane, which is 232.4 ± 0.4 kJ mol^{-1}.

TPES and mass-selected TPES in the molecular beam

The cooling in the molecular beam and the negligible background contribution are confirmed by the Ar TOF peak widths. Based on $T \approx 2018\frac{(Et_{FWHM})^2}{M}$ for a mass spectrum peak in 1st order space focus in a Wiley–McLaren-type time-of-flight spectrometer,[36] where T is the temperature in K, E the electric field in V cm^{-1}, t_{FWHM} the full width of the TOF peak at half maximum in μs, and M the molar mass in g mol^{-1}, the Ar peaks correspond to a translational temperature of 12 K. In contrast, the CH_3I^+ peak width at 12.15 eV, measured under the same circumstances, corresponds to 125 K translational temperature.

It is well established that Ar–CH_3I adducts and $(CH_3I)_n$, $n > 1$ dimers, trimers *etc.* may be formed in a molecular beam environment. Barry and Gorry found that at a nozzle temperature of 373 K and a backing pressure of 0.4 bar CH_3I, 8% of the pulsed molecular beam consists of dimers.[37] This has been corroborated by Donaldson, Vaida and Naaman, who derived an equilibrium constant for dimer formation in their experiment at room temperature of *ca.* 3 bar^{-1}.[38] Iodomethane dimers in a molecular beam have been directly observed by infrared spectroscopy after impacting them on a solid matrix.[39] Chen *et al.* expanded a 1 : 5 CH_3I : Ar mixture at 1 bar and measured the appearance potential of the dimer and trimer cations to be 9.19 ± 0.05 eV and 9.07 ± 0.10 eV, respectively.[40] Bogdanchikov *et al.*[41] calculated the neutral dimerization energy of the head-to-tail (HT) conformer to be −0.096 eV, and that of the head-to-head (HH) conformer to be −0.087 eV at the MP4(SDTQ)//MP2 level. The vertical and adiabatic ionization energies were calculated to be 9.74 *vs.* 9.42 eV (HT), and 9.51 *vs.* 8.44 eV (HH), respectively.[41] For reference, the ionization energy of CH_3I has been determined very accurately by two-photon zero electron kinetic energy (ZEKE) spectroscopy to be 9.538 eV.[42]

The total threshold photoelectron spectrum in the molecular beam with Ar as backing gas is shown as the solid points in Fig. 3a. In addition, several mass-selected TPES for $(CH_3I)_2^+$ (Fig. 3b), $ArCH_3I^+$, $Ar_2CH_3I^+$ and $Ar_3CH_3I^+$ (Fig. 3a) are also shown. The CH_3I vibrational structure in the total TPES is evident and the various peaks are readily assigned to known ion states, except for the significant peak at a 26 meV higher energy than the $^2E_{3/2}$ X monomer ground state ion peak, which does not correspond to a vibrational level of this ion. However, this peak is correlated with ions having the m/z of iodomethane. We attribute this peak to dissociative

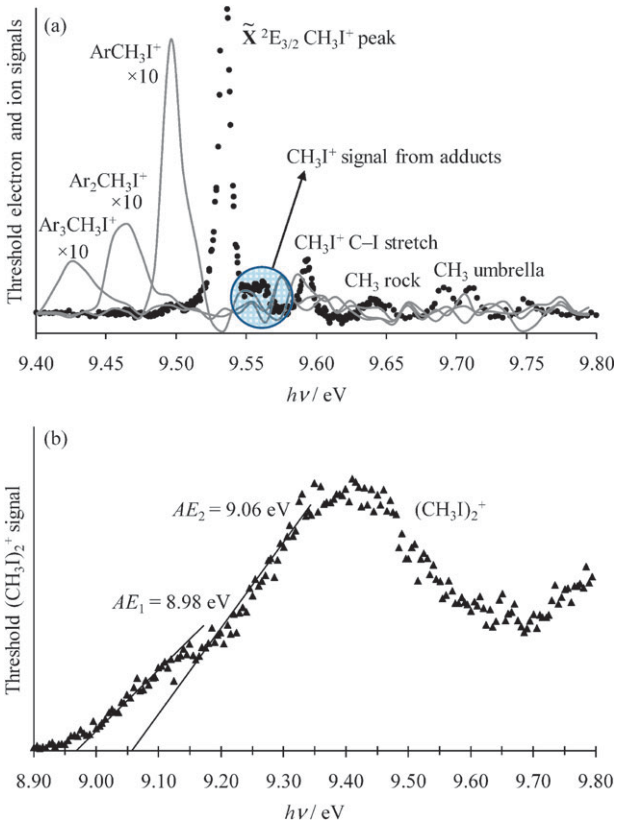

Fig. 3 Threshold photoelectron spectrum and mass-selected threshold photoelectron spectra for 2.5% CH_3I in Ar in the ionization energy region.

photoionization of CH_3I–Ar *via* CH_3I–Ar + $h\nu \rightarrow CH_3I^+ + Ar + e^-$, which means that this 26 meV shift is the binding energy of the neutral CH_3I–Ar dimer.

Turning now to the mass-selected TPES, we see a broad range of threshold cluster ion signal at energies below the CH_3I ionization energy. In particular, there are three peaks associated with the heterogeneous clusters, Ar_nCH_3I (n = 1, 2, 3). Because Ar is rather weakly bound to the iodomethane ion, the geometry does not change much. The 0–0 peak being dominant in the Franck–Condon distribution, peak positions are associated with adiabatic ionization energies. These are IE($ArCH_3I$) = 9.496 eV, IE(Ar_2CH_3I) = 9.466 eV, and IE(Ar_3CH_3I) = 9.425 eV. We note that the ionization energy for the $ArCH_3I$ adduct lies 40 meV below that of the monomer IE. We can combine this shift with the previously determined 26 meV neutral binding energy to derive the binding energy of the ion, which, therefore, is 40 + 26 = 66 meV.

At still lower energies, the mass-correlated TPES for the $(CH_3I)_2^+$ is shown in Fig. 3b. Because the neutral and ion dimers have different geometries, the TPES will not exhibit a sharp 0–0 peak but, rather, will be characterized by a broad Franck–Condon envelope. Dissociatively photoionized trimers are expected to have a small effect on the appearance energy of the dimer ion, since the mass-selected trimer signal is always negligible compared to the dimer one. If we assume that all of this signal corresponds to the process: $(CH_3I)_2 + h\nu \rightarrow (CH_3I)_2^+ + e^-$, and not to dissociative ionization of neutral trimers, we can interpret the two sloped regions as perhaps due

to ionization of two different dimer neutrals, namely the HH and HT conformers. Further calculations and experiments may be needed to unambiguously assign the dimer spectrum, but the dimer appearance energy is clearly below the previously reported value of 9.19 ± 0.05 eV.[40]

Breakdown diagram of CH_3I in a molecular beam

The breakdown diagram of CH_3I prepared in a molecular beam with Ar as backing gas, shown in Fig. 4, is shifted 20 meV to higher energies with respect to the room temperature data, similar to the PFI-PEPICO breakdown diagram published by Song *et al.*[10] In particular, the apparent onset energy, 12.268 eV is almost identical to the onset reported by Song *et al.* and the lingering parent ion signal above the onset energy is also observed in both experiments. Additionally, the A state energy levels are not nearly as conspicuous as in the room temperature breakdown diagram, nor is the width of the breakdown diagram consistent with the low temperature and sharp internal energy distribution expected in a molecular beam. The primary cause of these effects and the source of the disagreement between the apparent dissociation onset in the room temperature and molecular beam experiments is the formation of homogeneous and heterogeneous cluster ions as shown in Fig. 3.

An additional, independent reason for a broadened breakdown diagram may be different collection efficiencies for the parent and daughter ions. The collection efficiencies for CH_3I^+ and CH_3^+, which were 20 and 25% in the room temperature breakdown diagram, are reduced to 7 and 12% in the molecular beam, respectively, with Ar backing gas and the deflection plates on. The difference in the overall collection efficiencies is probably due to different collection volumes for electrons and ions as well as alignment issues, but it is also evident that CH_3I^+ ions formed in the molecular beam have a somewhat smaller chance of reaching the detector due to their larger initial transverse kinetic energy. When the different collection efficiencies are taken into account, the breakdown diagram narrows significantly, and the crossover energy (the photon energy at which the parent and daughter abundances are equally 50%) moves to be 17 meV higher in energy (Fig. 4).

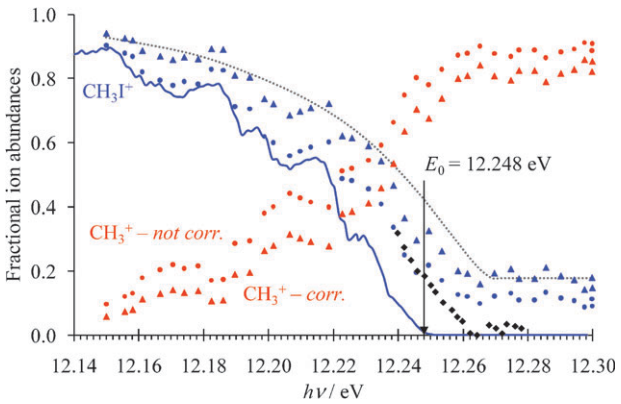

Fig. 4 Breakdown diagram of 2.5% CH_3I in the molecular beam with Ar as backing gas through a 30 μm nozzle. The fractional ion abundances are shown without (●) and with (▲) the correction for different collection efficiencies based on the ion signal ratio to the threshold electron signal (see text). The parent disappearance energy region is also shown for approx. 1 bar of Ar bubbling through room temperature CH_3I with a vapor pressure of 450 mbar through a 2 mm-long 50 μm nozzle (black ◆). The continuous line shows the fitted room temperature parent ion abundances. The dotted line shows the fitted breakdown curve of the parent ion in the molecular beam as reported by Song *et al.*[10]

The main reason for the smoothing of the breakdown diagram and the apparent high translational temperature of the parent CH_3I^+ ions, however, is that instead of the neutral CH_3I with very low rotational and vibrational internal energy, a mixture of clusters is ionized, which then dissociates and gives rise to CH_3I^+ with a wide internal energy distribution.

Neutral clusters shift the observed onset to higher energies because we cannot distinguish monomer ions, M^+, originating from dissociative threshold ionization of dimers ($M_2 + h\nu \rightarrow M^+ + M + e^-$) and direct ionization of a monomer ($M + h\nu \rightarrow M^+ + e^-$), as both M^+ ions are collected in coincidence with zero energy electrons. However, the disappearance of the M^+ ion is shifted to higher photon energy by the binding energy of the neutral dimer. The other consequence is that the M^+ peak width for the dissociative ionization is broader than that for the simple ionization of the monomer, which accounts for the higher translational temperature observed in the molecular beam data. The observed 20 meV shift in the parent ion disappearance (Fig. 4) is most likely a result of the CH_3I–Ar dimers because, as reported by Bogdanchikov *et al.*,[41] the iodomethane dimer binding energy is calculated to be about 100 meV, which is too large to account for the small shift in the breakdown diagram. On the other hand, the measured 26 meV binding energy of Ar-tagged CH_3I (see Fig. 3), provides an explanation for the shift in the onset energy in the molecular beam. The lingering parent ion signal at high energies can then be explained by the dissociative photoionization of the methyl iodide dimers and multimers, which produce monomer CH_3I^+ ions with at least 100 meV less internal energy than the corresponding ions stemming from monomer neutrals. These parent ions will not dissociate in the photon energy range of the breakdown diagram, and give rise to the lingering parent ion signal.

We have also tried to increase the iodomethane concentration in the beam by bubbling Ar through CH_3I, which has a vapor pressure of about 450 mbar at room temperature, and employed a thicker, 2 mm-long nozzle with a 50 μm nozzle diameter. However, as shown by the diamonds in Fig. 4, the observed breakdown diagram shift decreased (when the two correction efficiency corrected data sets are compared), and the lingering parent ion signal disappeared. Since these conditions are very similar to the ones in the experiment of Song *et al.*, with the exception of the change in the nozzle geometry, we attribute the diminished adduct formation to the effect of the nozzle.

To elucidate these effects further, the breakdown diagram of iodomethane was also obtained in 2.5% concentration with Ne as backing gas and with the long, 50 μm nozzle. The breakdown diagram was very similar to the one obtained with the 50 μm nozzle and Ar as a backing gas, which can be a nozzle effect and/or indicative of the smaller binding energy of Ne to CH_3I.

Electric field (Stark) effects

In order to detect ions with high collection efficiencies, especially in the case of a molecular beam sample where the neutrals have significant velocities perpendicular to the extraction axis, it is essential to extract the ions with a substantial electric field. This raises concerns about Stark shifts in measuring dissociation onsets in ions. Chupka has shown that an approximate expression for the shift in the ionization energy in the diabatic limit is

$$6\,\mathrm{cm}^{-1}\sqrt{F/(\mathrm{V\,cm}^{-1})}, \qquad (1)$$

where F is the electric field.[43] This translates into shifts of 27 to 66 cm^{-1} for electric fields of 20 and 120 V cm^{-1}, respectively, which is several times the accuracy (8 cm^{-1}) we strive for in terms of onset energies.

The Ar TPES was obtained for the ground $^2P_{3/2}$ and $^2P_{1/2}$ states at 20, 80, and 120 V cm^{-1} electric fields. To minimize the effects of the photon energy resolution and other experimental uncertainties in determining the ionization onsets, the apparent ionization onsets were shifted by a constant between 2 and 12 cm^{-1} for each state with respect to the known ionization energies,[44–46] to ensure the best possible square root dependence of the Stark shift on the field. Table 1 lists the results for Ar obtained at three different field strengths and similar results for several states in the N_2 TPES obtained at 20 and 120 V cm^{-1}. The average prefactor weighted by the number of experimental points is 5.98 cm^{-1}, in excellent agreement with eqn (1). These results also agree well with a photoionization onset measurement in N_2 reported by Berkowitz and Ruscic,[47] where they found a value of 6.1 cm^{-1}.

Less well documented are possible Stark effects in dissociation onset measurements. In order to correct for any lowering of dissociation onset measurements due to Stark effects, we collected data at various electric fields from 20 to 120 V cm^{-1} for both the H loss from the methane ion and I loss from iodomethane ion (Fig. 5). A spline fit was applied to the experimental data points, the TPES intensities were re-normalized, and the curves were shifted in energy to get the best overlap between the low field and the high field data. The structureless CH_4 TPES is best fitted without a shift. The differences are clearest for the CH_3I TPES, for which the 120 V cm^{-1} curve needs to be shifted 2.4 meV, which improves the overlap to a great degree. The breakdown diagram is shifted 1.9 meV to higher energies, mainly because of the shifts in the A peaks. The CH_3^+ onset energy (*i.e.* the disappearance energy of the CH_3I^+ parent ion), however, remains unchanged at different fields. This indicates that if Rydberg states are involved in the dissociative ionization process, their decay rates toward a variety of reaction products are faster than the rate of field ionization.

Table 1 Experimental prefactors for the Stark shift in the ionization onsets of Ar and N_2

Ionization process	Prefactor/cm^{-1}
$Ar^+\ ^2P_{3/2} \leftarrow Ar\ ^1S_0$	6.7
$Ar^+\ ^2P_{1/2} \leftarrow Ar\ ^1S_0$	6.2
$N_2^+\ X\ (v^+ = 0) \leftarrow N_2\ X\ (v'' = 0)$	5.5
$N_2^+\ X\ ^2\Sigma_g^+ (v^+ = 1) \leftarrow N_2\ X\ ^1\Sigma_g^+ (v'' = 0)$	5.8
$N_2^+\ A\ (v^+ = 0) \leftarrow N_2\ X\ (v'' = 0)$	6.2
$N_2^+\ A\ (v^+ = 1) \leftarrow N_2\ X\ (v'' = 0)$	5.0

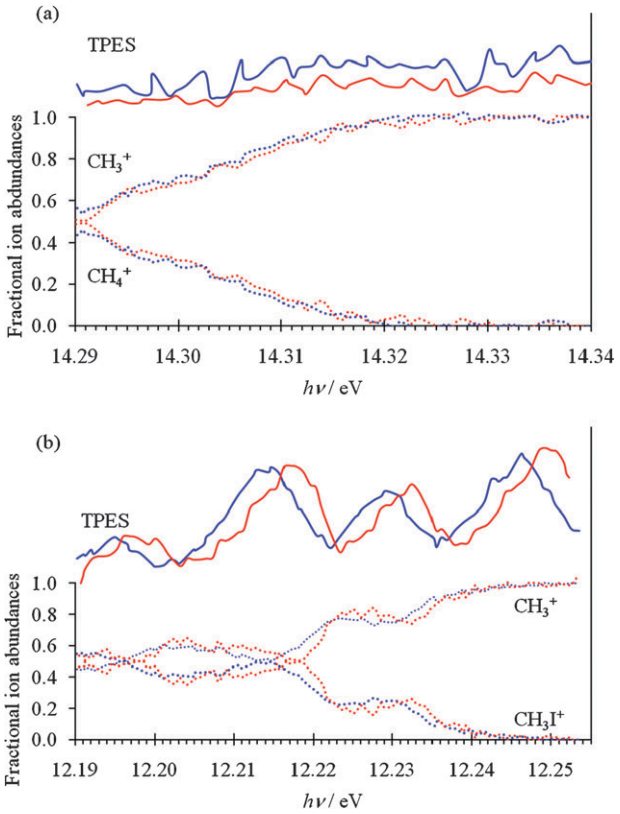

Fig. 5 Field effects in the breakdown diagram of (a) CH_4 (blue: 120 V cm^{-1}, red: 40 V cm^{-1}) and (b) CH_3I (blue: 120 V cm^{-1}, red: 20 V cm^{-1}). Fitted energy shifts to maximize the TPES and breakdown diagram overlap between the high field and the low field data are 0, 1.5 meV, 2.4 meV and 1.9 meV for CH_4 TPES, CH_4 breakdown diagram, CH_3I TPES, CH_3I breakdown diagram, respectively. The CH_3^+ onset energy in CH_3I, however, is independent of the field.

Some time ago, Weitzel *et al.*[48] proposed a mechanism for pulsed field ionization in the vicinity of dissociation onsets, in order to account for the observation of steps in the threshold electron yield. This mechanism invoked the participation of long-lived Rydberg states. This points to a different ionization mechanism in constant field (DC) PEPICO and PFI-PEPICO. In the former, we rely on fast autoionization from dissociative neutral states, and model the dissociation as taking place on the ion surface, whereas in the model of Weitzel *et al.*, the dissociation is described as taking place on the Rydberg surface, and field ionization follows when the pulse is applied. The fact that no steps are observed in our threshold electron spectra supports the argument that dissociative photoionization proceeds *via* different channels in the two experiments.

Conclusions

Imaging photoelectron photoion coincidence spectroscopy (iPEPICO) has been used to construct a breakdown diagram in order to determine the dissociative photoionization

onset for CH_3^+ + I production. The 0 K onset energy of 12.248 ± 0.003 eV obtained with a room temperature sample can be used in conjunction with very accurate methyl ion and I atom heats of formation to determine a $\Delta_f H^o_{298\ K}(CH_3I)$ = 15.23 ± 0.3 kJ mol^{-1}, and also with the methyl radical ionization energy to determine the C–I bond energy in CH_3I to be 232.4 ± 0.4 kJ mol^{-1}. The breakdown diagram and ion yield spectra exhibit A state structure on top of a larger continuum of states, which indicates that the total iodomethane ion yield consists of excitation to short-lived Rydberg states that convert to X states *via* the mechanism proposed by Guyon *et al.* and Chupka *et al.* and also to long-lived Rydberg states with less rotational energy that undergo field ionization to the A ion state and then internal conversion to vibrationally excited X states. Field ionization is shown to be a marginal process when ionizing molecules are close to a dissociation onset, as the excited neutrals autoionize rapidly as soon as the nuclear geometry permits. This is found to be the case for CH_3I, where dissociative photoionization takes place in a Frank–Condon disallowed region, as well as for CH_4, where the Frank–Condon factors are non-zero in the H-loss photon energy range. Thus, DC electric fields are not expected to have an effect on the measured dissociation onset of internal energy selected ions.

The breakdown diagram of a molecular beam sample (2.5% CH_3I in Ar or Ne) could not be interpreted quantitatively. As found in a previous molecular beam study, the crossover region was not sharp as expected for a cold sample, and the parent ion signal lingered on at energies well in excess of the dissociation limit. iPEPICO ion yields near the ionization onset provided the explanation. Numerous homogeneous, $(CH_3I)_n$, as well as heterogeneous, $(CH_3I)_nAr_m$, clusters contaminated the beam, all of which contributed to both CH_3I^+ and CH_3^+ signals. The only means of differentiating the true parent ions from those formed by dissociative photoionization is by the time-of-flight peak width, which is sensitive to the kinetic energy of the molecule. The result of these clusters is to shift the observed fragmentation onset to higher energies by about 20 meV. The mass analyzed TPES for heterogenous CH_3I–Ar_n clusters yielded ionization energies of 9.496 eV (Ar–CH_3I), 9.466 eV (Ar_2–CH_3I), and 9.425 eV (Ar_3–CH_3I), and binding energies for Ar–CH_3I of 26 meV and for Ar–CH_3I^+ of 66 meV.

Acknowledgements

We are grateful to Richard P. Tuckett for the fluorescence measurement. This work was funded by the Swiss Federal Office of Energy (BFE contract number 101969/152433), the US Department of Energy (DOE Grant DE-FG02-97ER14776), and the US National Science Foundation.

References

1 A. Karton, A. Tarnopolsky, J.-F. Lamere, G. C. Schatz and J. M. L. Martin, *J. Phys. Chem. A*, 2008, **112**, 12868–12886.
2 A. Karton, E. Rabinovich, J. M. L. Martin and B. Ruscic, *J. Chem. Phys.*, 2006, **125**, 144108–144124.
3 M. E. Harding, J. Vazquez, B. Ruscic, A. K. Wilson, J. Gauss and J. F. Stanton, *J. Chem. Phys.*, 2008, **128**, 114111–114125.
4 A. Bodi, M. Johnson, T. Gerber, Z. Gengeliczki, B. Sztáray and T. Baer, *Rev. Sci. Instrum.*, 2009, **80**, 034101–034107.
5 G. K. Jarvis, K. M. Weitzel, M. Malow, T. Baer, Y. Song and C. Y. Ng, *Rev. Sci. Instrum.*, 1999, **70**, 3892–3906.
6 K.-C. Lau and C. Y. Ng, *Acc. Chem. Res.*, 2006, **39**, 823–829.
7 G. A. Garcia, H. Soldi-Lose and L. Nahon, *Rev. Sci. Instrum.*, 2009, **80**, 023102–023113.
8 B. P. Tsai, T. Baer, A. S. Werner and S. F. Lin, *J. Phys. Chem.*, 1975, **79**, 570–574.
9 J. C. Traeger and R. G. McLoughlin, *J. Am. Chem. Soc.*, 1981, **103**, 3647–3652.
10 Y. Song, X.-M. Qian, K.-C. Lau and C. Y. Ng, *J. Chem. Phys.*, 2001, **115**, 4095–5003.
11 K. M. Weitzel and F. Güthe, *Chem. Phys. Lett.*, 1996, **251**, 295–300.
12 S. P. Goss, J. D. Morrison and D. L. Smith, *J. Chem. Phys.*, 1981, **75**, 757–762.
13 D. C. McGilvery and J. D. Morrison, *J. Chem. Phys.*, 1977, **67**, 368–369.
14 K. Walter, R. Weinkauf, U. Boesl and E. W. Schlag, *J. Chem. Phys.*, 1988, **89**, 1914–1922.
15 M. Lee and M. S. Kim, *J. Chem. Phys.*, 2007, **127**, 124313–124316.
16 Y. J. Bae and M. S. Kim, *ChemPhysChem*, 2008, **9**, 1709–1714.
17 Y. J. Bae and M. S. Kim, *J. Chem. Phys.*, 2008, **128**, 124324–124330.
18 A. Bodi, B. Sztáray, T. Baer, M. Johnson and T. Gerber, *Rev. Sci. Instrum.*, 2007, **78**, 084102–084108.
19 M. Johnson, A. Bodi, L. Schulz and T. Gerber, *Nucl. Instrum. Methods Phys. Res., Sect. A*, 2009, DOI: 10.1016/j.nima.2009.08.069.
20 Y. Ralchenku, A. E. Kramida and J. Reader, and NIST ASD Team (2008), *NIST Atomic Spectra Database*, National Institute of Standards and Technology, Gaithersburg, MD, 2008 p. available: http://physics.nist.gov/asd3.
21 B. Sztáray and T. Baer, *Rev. Sci. Instrum.*, 2003, **74**, 3763–3768.
22 I. Nenner, P. M. Guyon, T. Baer and T. R. Govers, *J. Chem. Phys.*, 1980, **72**, 6587–6592.
23 P. M. Guyon, W. A. Chupka and J. Berkowitz, *J. Chem. Phys.*, 1976, **64**, 1419–1436.
24 A. C. Parr, A. J. Jason and R. Stockbauer, *Int. J. Mass Spectrom. Ion Phys.*, 1978, **26**, 23–38.
25 A. C. Parr, A. J. Jason, R. Stockbauer and K. E. McCulloh, *Int. J. Mass Spectrom. Ion Phys.*, 1979, **30**, 319–330.
26 A. C. Parr, A. J. Jason and R. Stockbauer, *Int. J. Mass Spectrom. Ion Phys.*, 1980, **33**, 243–251.
27 E. A. Fogleman, H. Koizumi, J. P. Kercher, B. Sztáray and T. Baer, *J. Phys. Chem. A*, 2004, **108**, 5288–5294.
28 P. M. Guyon, T. Baer and I. Nenner, *J. Chem. Phys.*, 1983, **78**, 3665–3672.
29 W. A. Chupka, P. J. Miller and E. E. Eyler, *J. Chem. Phys.*, 1988, **88**, 3032–3036.
30 T. Baer, B. Sztáray, J. P. Kercher, A. F. Lago, A. Bodi, C. Scull and D. Palathinkal, *Phys. Chem. Chem. Phys.*, 2005, **7**, 1507–1513.
31 R. P. Tuckett, personal communication, 2008.
32 B. Ruscic, R. E. Pinzon, M. L. Morton, G. Laszevski, S. J. Bittner, S. G. Nijsure, K. A. Amin, M. Minkoff and A. F. Wagner, *J. Phys. Chem. A*, 2004, **108**, 9979–9997.
33 K. M. Weitzel, M. Malow, G. K. Jarvis, T. Baer, Y. Song and C. Y. Ng, *J. Chem. Phys.*, 1999, **111**, 8267–8270.
34 J. B. Pedley, *Thermochemical Data and Structures of Organic Compounds*, Thermodynamics Research Center, College Station, 1994.
35 B. Ruscic, J. E. Boggs, A. Burcat, A. G. Császár, J. Demaison, R. Janoschek, J. M. L. Martin, M. L. Morton, M. J. Rossi, J. F. Stanton, P. G. Szalay, P. R. Westmoreland, F. Zabel and T. Berces, *J. Phys. Chem. Ref. Data*, 2005, **34**, 573–656.
36 T. Baer and W. L. Hase, *Unimolecular Reaction Dynamics: Theory and Experiments*, Oxford University Press, New York, 1996, p. 162.
37 M. D. Barry and P. A. Gorry, *Mol. Phys.*, 1984, **52**, 461–473.
38 D. J. Donaldson, V. Vaida and R. Naaman, *J. Chem. Phys.*, 1987, **87**, 2522–2530.
39 F. Ito, T. Nakanaga, Y. Futami, S. Kudoh, M. Takayanagi and M. Nakata, *Chem. Phys. Lett.*, 2001, **343**, 185–191.

40 J. Chen, L. Pei, J. Shu, C. Chen, X. Ma, L. Shen and Y. Zhang, *Chem. Phys. Lett*., 2001, **345**, 57–64.
41 G. A. Bogdanchikov, A. V. Baklanov and D. H. Parker, *Chem. Phys. Lett*., 2003, **376**, 395–402.
42 B. Urban and V. E. Bondybey, *J. Chem. Phys*., 2002, **116**, 4938–4947.
43 W. A. Chupka, *J. Chem. Phys*., 1993, **98**, 4520–4530.
44 J. W. Hepburn, *J. Chem. Phys*., 1997, **107**, 7106–7113.
45 I. Velchev, W. Hogervorst and W. Ubachs, *J. Phys. B: At., Mol. Opt. Phys*., 1999, **32**, L511–L516.
46 C. Yamada, H. Kanamori and E. Hirota, *J. Chem. Phys*., 1985, **83**, 552–555.
47 J. Berkowitz and B. Ruscic, *J. Chem. Phys*., 1990, **93**, 1741–1746.
48 K. M. Weitzel, G. K. Jarvis, M. Malow, T. Baer, Y. Song and C. Y. Ng, *Phys. Rev. Lett*., 2001, **86**, 3526–3529.